

In Situ Study of Colloid Crystallization in Constrained Geometry

Robert Kori Golding, Patrick C. Lewis, and Eugenia Kumacheva*

*Department of Chemistry, University of Toronto, 80 Saint George Street,
Toronto, Ontario M5S 3H6, Canada*

Mathieu Allard and Edward H. Sargent

*Department of Electrical and Computer Engineering, University of Toronto,
10 King's College Road, Toronto, Ontario M5S 3G4, Canada*

Received April 7, 2003. In Final Form: August 27, 2003

We visualized in real time electrodeposition-driven colloid crystal growth on patterned conductive surfaces. The electrode was patterned with dielectric ribs and conductive grooves; the groove width was commensurate or incommensurate with a two-dimensional colloid crystal lattice. Electrodeposition was carried out against gravity to decouple sedimentation and electrodeposition of colloid particles. Our experiments reveal the following: (i) Colloid crystal growth occurs under the action of electrohydrodynamic forces, in contrast with colloid assembly under the action of capillary forces. (ii) Confinement of the colloid arrays reduces the size of particle clusters. Small clusters easily undergo structural rearrangements to produce close-packed crystals when the groove width is commensurate or nearly commensurate with the 2D lattice. (iii) Incommensurability between the two-dimensional crystalline lattice and the groove width exceeding ca. 15% leads to the formation of non-close-packed structures and the distortion of colloid arrays.

Over the past decade or so, assembly of submicrometer particles in two- and three-dimensional colloid arrays has generated a revived interest due to the potential applications of these arrays in the fabrication of photonic band gap materials.¹ Previously, colloid crystal growth was governed by gravity and capillary forces,² or it was assisted by oscillatory shear or electric or magnetic fields.^{3–5} Generally, these methods led to the formation of polycrystalline structures: the quality of colloid crystal was determined by the dimensions of the coexisting periodic domains. Lately, several groups have reported a significant enhancement of colloid crystallization in constrained geometries, that is, on substrates patterned with *planar*^{6–8} or *topographic* patterns.^{9–12} These methods relied on submicrometer- or micrometer-size surface features: in

the first case, the characteristic size of the pattern was commensurate with a *single* particle diameter, in the second case, it was on the order of *several* particle diameters. In planar patterning,^{6–8} the surface was chemically patterned with self-assembled monolayers producing isolated ionic and cationic regions. Negatively charged colloid particles were electrostatically deposited from their aqueous dispersions onto the cationic surface domains. During the stage of drying, the lateral capillary forces acting between the particles brought them together and, under particular conditions, generated a reasonable extent of order in the 2D colloid arrays. The topographic patterning used for colloidal epitaxy¹² did not rely on a specific attraction force between the particles and the substrate. The substrate relief (voids or microchannels) led to predetermined particle assembly by physical means during microbead sedimentation or evaporation of liquid from the dispersion.⁹ In the stage of drying of particle arrays, colloid crystallization occurred due to capillary forces acting between the beads.

Recently, our group reported colloid crystal growth driven by electrodeposition on patterned substrates.¹³ Our experiments were motivated by the relatively high speed of colloid electrodeposition (by contrast with sedimentation), though the resulting particle arrays on nonpatterned substrates had a polycrystalline structure (similar to that obtained in particle sedimentation). We note, however, that in most of electrodeposition experiments, particle assembly was in the same direction as the influence of gravity.^{4,14–16} In our work,¹³ electrodeposition on patterned surfaces was conducted against gravity: negatively charged particles moved under the action of electric field

- (1) John, S. *Phys. Rev. Lett.* **1987**, *58*, 2486.
- (2) Davis, K. E.; Russel, W. B.; Glantschnig, W. J. *J. Chem. Soc., Faraday Trans.* **1991**, *87*, 411. (b) Holland, B. T.; Blanford, C. F.; Stein, A. *Science* **1998**, *281*, 538. (c) Jiang, P.; Bertone, J. F.; Hwang, K. S.; Colvin, V. L. *Chem. Mater.* **1999**, *11*, 2132.
- (3) Vickreva, O.; Kalinina, O.; Kumacheva, E. *Adv. Mater.* **2000**, *12*, 110.
- (4) Rogach, A. L.; Kotov, N. A.; Koktysh, D. S.; Ostrander, J. W.; Ragoisha, G. A. *Chem. Mater.* **2000**, *12*, 2721. (b) Holdado, M.; Garsia-Santamaria, F.; Blanco, A.; Ibisate, M.; Cintas, A.; Miguez, H.; Serna, C. J.; Molpceres, C.; Requena, J.; Mifsud, A.; Meseguer, F.; Lopez, C. *Langmuir* **1999**, *15*, 4701.
- (5) Xu, X. L.; Majetich, S. A.; Asher, S. A. *J. Am. Chem. Soc.* **2002**, *124*, 13864.
- (6) Tien, J.; Terfort, A.; Whitesides, G. M. *Langmuir* **1997**, *13*, 5349.
- (7) Aizenberg, J.; Braun, P. V.; Wiltzius, P. *Phys. Rev. Lett.* **2000**, *84*, 2997.
- (8) Chen, K. M.; Jiang, X.; Kimerling, L. C.; Hammond, P. *Langmuir* **2000**, *26*, 7825.
- (9) van Blaaderen, A.; Rue, R.; Wiltzius, P. *Nature* **1997**, *385*, 321. (b) van Blaaderen, A.; Hoogenboom, J. P.; Vossen, D. L. J.; Yethiraj, A.; van der Horst, A.; Visscher, K.; Dogterom, M. *Faraday Discuss.* **2003**, *123*, 107. (c) Hoogenboom, J. P.; Yethiraj, A.; van Langen-Suurling, A. K.; Romijn, J.; van Blaaderen, A. *Phys. Rev. Lett.* **2002**, *89*, 256104.
- (10) Lin, K.; Crocker, J. C.; Prasad, V.; Schofield, A.; Weitz, D. A.; Lubensky, T. C.; Yodh, A. G. *Phys. Rev. Lett.* **2000**, *85*, 1770.
- (11) Yi, D. K.; Seo, E.-M.; Kim, D.-Y. *Appl. Phys. Lett.* **2002**, *80*, 225.
- (12) Yin, Y.; Lu, Y.; Gates, B.; Xia, Y. *J. Am. Chem. Soc.* **2001**, *123*, 8718; (b) Ozin, G. A.; Yang, S. M. *Adv. Funct. Mater.* **2001**, *11*, 95.

- (13) Kumacheva, E.; Golding, R. K.; Allard, M.; Sargent, E. H. *Adv. Mater.* **2002**, *14*, 221.
- (14) Trau, M.; Saville, D. A.; Aksay, I. A. *Science* **1996**, *272*, 706. (b) Trau, M.; Saville, D. A.; Aksay, I. A. *Langmuir* **1997**, *13*, 6375.
- (15) Solomentsev, Y.; Bohmer, M.; Anderson, J. L. *Langmuir* **1997**, *13*, 6058.
- (16) Bohmer, M. *Langmuir* **1996**, *12*, 5747.

upward—toward the anode. The surface of the anode was patterned with conductive grooves and dielectric ridges. Submicrometer polymer microbeads electrodeposited in the conductive grooves *and* were physically confined by the rigid walls. Thus the strategy employed both attraction between the particles and the substrate and physical confinement.

Here, we seek to gain understanding of the mechanism of particle assembly in a constrained geometry. We conducted real-time studies of colloid crystallization under the action of an electric field. Our objectives were 2-fold. First, we examined the sequence of steps in which colloid particles deposited in the conductive grooves formed a crystal. Second, we explored the role of commensurability between the width of confining grooves and the two-dimensional lattices formed by the microbeads. To the best of our knowledge, the only *in situ* study of colloid crystallization in confined geometry was reported by Xia et al.^{12a} for particle assembly driven by the combination of physical templating and capillary forces.

Experimental Section

Sample Preparation. Aqueous dispersions of negatively charged polystyrene microspheres with average diameters of 3.88 and 5.0 μm were obtained from Professor Manners Group (University of Toronto) and Bangs Laboratories, respectively. The particle polydispersity index was ca. 1.3. The dispersions were dialyzed against deionized water and diluted with ethanol to obtain a 50/50 volume mixture of water and ethanol. The concentration of polymer particles in the dispersion varied from 0.0025 to 0.025 wt %.

The patterning of the anode surface was realized by writing holographic gratings in positive photoresist layers (Shipley Microresist S1827, thickness ca. 2 μm), spin-coated on glass slides coated with indium tin oxide (ITO). A helium–cadmium laser (35 mW continuous beam at 442 nm) was used for writing. Exposure followed by the development of the photoresist produced a pattern of periodically alternating isolating ribs and conductive grooves on the surface of ITO-covered slides. The width of the grooves, L , was varied from ca. 4.0 to 19 μm by changing the angle between the two interfering beams.

Electrodeposition Experiments. Two glass slides (2.5 \times 2.5 cm) coated with 200 nm ITO coating were used as optically transparent electrodes. The top electrode (anode) was patterned with dielectric ribs and conductive grooves (see above). The electrodes were separated by 5 mm Teflon spacers. Once the colloid dispersion was placed into the electrodeposition cell, the latter was sealed and mounted on the platform of the optical microscope. Particle electrodeposition was studied with a Zeiss Axioplan 40 microscope, using an AxioCam MR digital camera. The images were captured every 30 s and then subjected to image analysis. The electrodeposition experiments were conducted in a potentiostatic regime at 20 V (40 V/cm electric field).

Results

Prior to electrodeposition on patterned surfaces, the assembly of polystyrene microbeads under the action of electric field was examined for the nonpatterned ITO-coated substrates. Since the force imposed on the particles by the electric field counteracted the gravity force, a substantially higher electric field than that used in the previous studies^{4,14–16} was employed. When no potential was applied to the electrodes, the anode (top electrode) remained blank, whereas upon the application of a 20 V dc field, the negatively charged colloids began to rise toward the positively charged electrode.

The characteristic features of electrodeposition on a nonpatterned surface were akin to those previously described.^{14–16} Colloid assembly followed a three-stage process. In the initial nucleation stage, the individual particles randomly deposited on the anode (gaseous state),

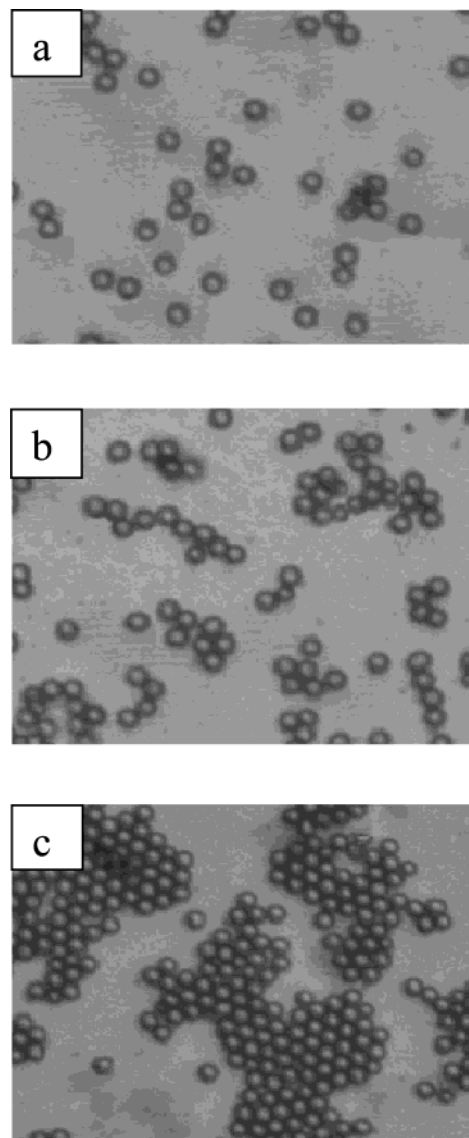


Figure 1. Colloid arrays obtained by electrodeposition on nonpatterned ITO substrates for 3.88 μm size beads at potential 20 V. Times of electrodeposition were (a) 30, (b) 90, and (c) 210 s.

as shown in Figure 1a. Following their deposition, the microbeads moved laterally on the electrode surface. In the second stage, with increase of surface coverage, the particles formed diads and triads, which merged to form small clusters (liquid phase) (Figure 1b). Attraction between the beads appeared when the distance between them was on the order of several particle diameters. The individual colloids and small particle clusters moved readily across the surface of the electrode until they produced an immobile cluster with a critical number of particles (generally, about 15–20 particles). In the third stage, particle clusters began to merge to form large two-dimensional (2D) islands (“crystalline phase”), shown in Figure 1c. Crystallization occurred either through the collisions of small microbead clusters or via the deposition of individual particles between the immobilized clusters. The islands continued to grow and merge until no more colloids in the dispersion were available for deposition. When the particle concentration in the dispersion exceeded 0.005 wt %, the colloids often preferentially deposited on already-deposited particles, despite the fact that uncoated conductive fragments existed on the surface of the anode. This feature was earlier observed by Solomentsev et al.¹⁵

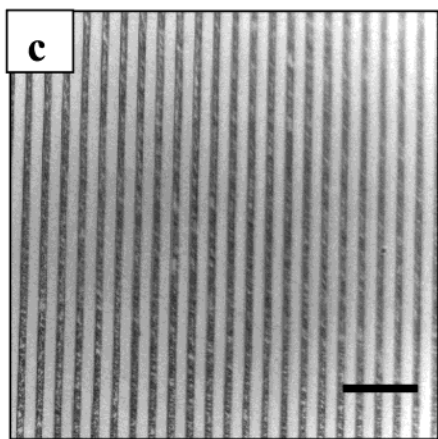
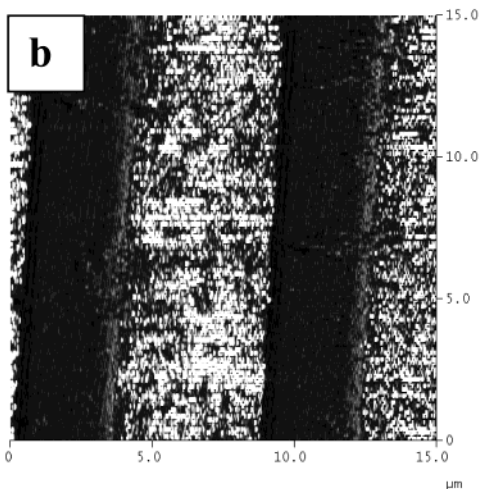
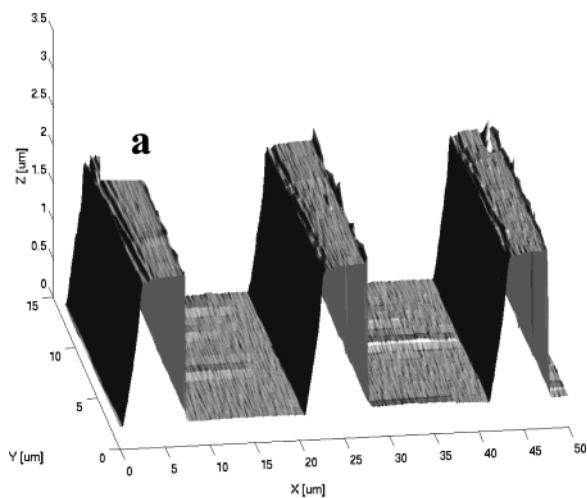


Figure 2. (a) Surface profile of the samples used for deposition, measured by an atomic force microscope (AFM). For these samples, the groove width and height are 13.8 and 2.0 μm , respectively. (b) Conductivity of the patterned substrate, measured by a current-sensing AFM. The bright areas are conductive, the dark ones are insulating. (c) SEM micrograph of the patterned surface. Scale bar is 40 μm .

Following the reversal of the electric field, the deposited microbeads detached from the surface and moved toward the bottom electrode.

Following these experiments, we conducted electrodeposition on the microspheres on patterned surfaces. The current-sensing atomic force microscope (AFM) (Digital Instruments) and scanning electron microscopy (SEM) image of the patterned substrate are shown in Figure 2.

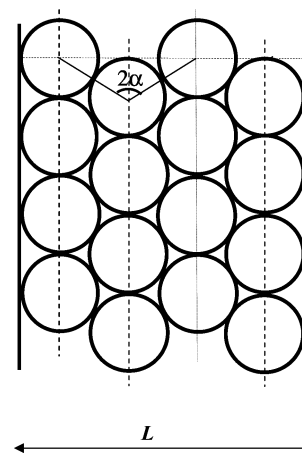


Figure 3. Schematic of a two-dimensional hexagonal lattice formed by colloid spheres with radius R in the groove of width L . Angle 2α is 120° .

The bottom of the conductive groove had a root mean square roughness not exceeding several nanometers, similar to the roughness of the surface of the uncoated ITO slides. The surface profile reveals equally spaced photoresist ribs with smooth vertical walls, separated by grooves in which the ITO is exposed. This is confirmed by the surface conductivity profile which shows that the entire area of the grooves is conductive; the speckle pattern in the conductivity reflects the grain structure of the ITO. The grooves exhibited a small variation in width, due to unequal exposure of the resist. Away from the edges of the grating, the width of the groove varied by no more than 7%.

The effect of commensurability between the groove width and the microsphere size was examined in terms of the ratio $L/2R$, where L is the lateral distance between the two insulating walls and R is the particle radius. For the hexagonal close-packed 2D lattice shown in Figure 3

$$L/2R = [(n - 1) \sin 60^\circ + 1] \quad (1)$$

where n is the number of layers aligned parallel to the groove wall (shown with the dotted lines in Figure 3). Later in the text we refer to these layers as “columns”. It follows from eq 1 that $L/2R$ is 1.0, 1.87, 2.73, 3.60, and 4.64 for one, two, three, four, and five columns, respectively. Figures 4–6 show the representative images of the colloid arrays deposited in the conductive grooves with various $L/2R$. In parts a and c–e of Figure 4, the width of the grooves is commensurate or nearly commensurate with the 2D close-packed lattices of 3.88 μm size beads, that is, the experimental ratio of the width of the groove to the particle diameter, $L/2R_{\text{exp}}$, is close to that anticipated from eq 1: (a) 1.03, (c) 2.87, (d) 3.56, and (e) 4.7. The corresponding colloid arrays exhibit the features of a hexagonal close-packed structure. Figure 4b shows the arrays of 5 μm size beads: for $L/2R_{\text{exp}} = 1.55$ ($L/2R = 1.87$). The difference between the two ratios occurred because in this case the groove height was slightly smaller than the particle diameter (2 μm vs 5 μm); thus the deposited particles were weakly confined by the ridges and could occupy a larger area.¹⁷

When the width of the grooves was incommensurate with the hexagonal lattice, e.g., when the value of $L/2R_{\text{exp}}$ exceeded $L/2R$ by more than ca. 15%, several types of

(17) Decrease of the ridge height to less than ca. 20% of the particle diameter led to the insufficient confinement of the beads: the edge of the colloid crystal became wavy and the appearance of the array was similar to that observed in the case of planar patterning (refs 7 and 8).

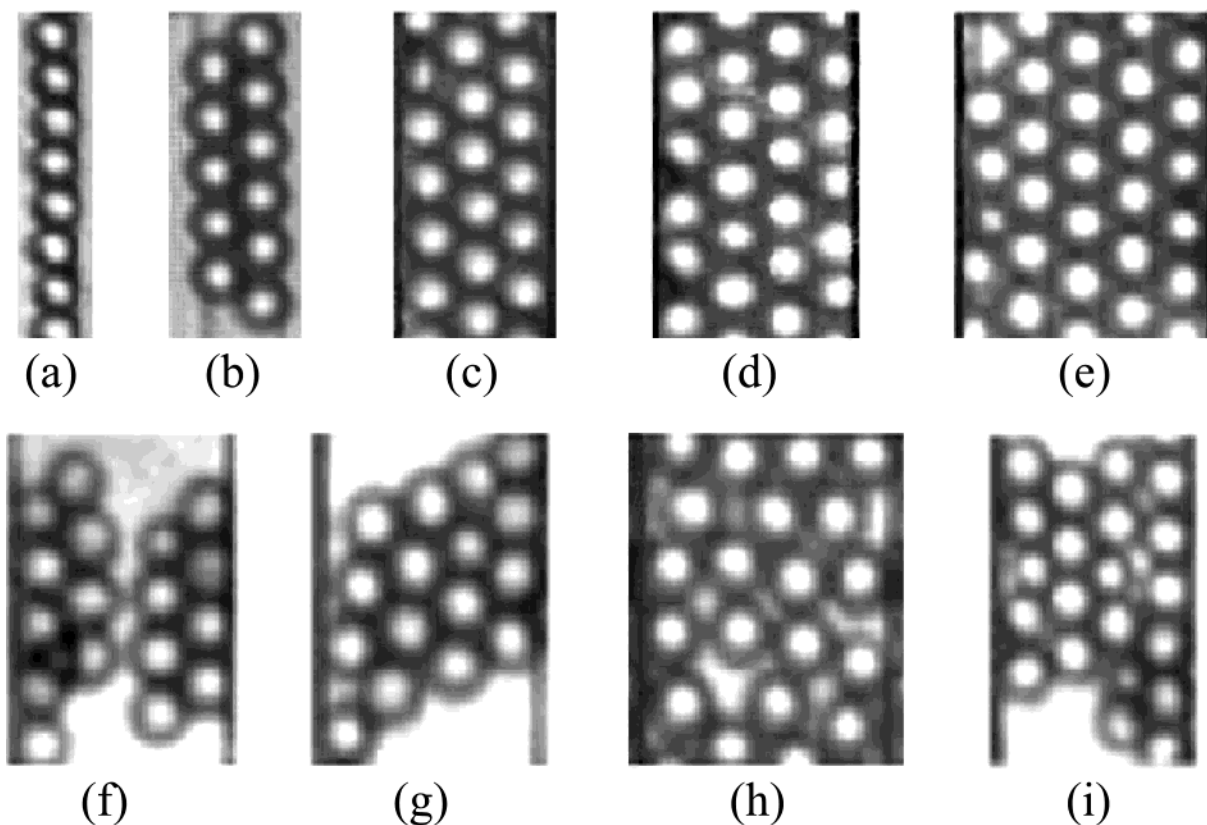


Figure 4. Effect of commensurability and incommensurability on electrodeposition of colloid particles in grooves with varying width. In images (a–e) $L/2R_{\text{exp}}$ (see text) is equal to or is very close to $L/2R$ calculated from eq 1. L/R_{exp} : (a) 1.03, (b) 1.55, (c) 2.87, (d) 3.56, (e) 4.7. In images (f and g) the deviation between $L/2R_{\text{exp}}$ and $L/2R$ exceeds 15%. L/R : (f) 4.26, (g) 4.26, (h) 4.96. Image (i) shows the effect of particle polydispersity when $L/R_{\text{exp}} = 3.56$.

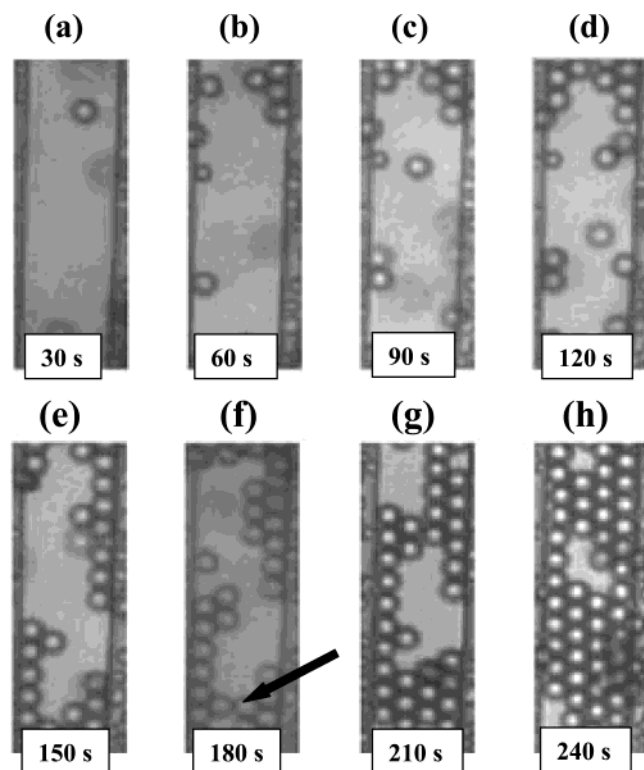


Figure 5. Kinetics of colloid assembly during electrodeposition of $3.88 \mu\text{m}$ size spheres in $13.8 \mu\text{m}$ wide conductive grooves.

particle assemblies were observed. Parts f and g of Figure 4 show four columns of $3.88 \mu\text{m}$ size beads deposited in

a $16.5 \mu\text{m}$ wide groove ($L/2R_{\text{exp}} = 4.26$; $L/2R = 3.60$). In Figure 4f, the two-column arrays adjacent to the groove walls have a close-packed structure; the gap between them, however, has an insufficient width to accommodate another column of particles. In Figure 4g, a close-packed particle array is skewed; in this case, the gap exists between the groove wall and the adjacent particle column. Occasionally, for $L/2R_{\text{exp}} > L/2R$, non-close-packed particle arrays were formed, shown in Figure 4h. Microbead polydispersity strongly influenced particle assembly; in Figure 4i embedding of small particles in the colloid array ($L/2R_{\text{exp}} = 3.56$, $n = 4$) distorted the 2D lattice.

To follow the kinetics of 2D crystallization, a series of images were captured during particle deposition from the same spot on the substrate (Figure 5). In the initial stage (Figure 5a), the microbeads deposited in the groove randomly, similar to the deposition on unpatterned surfaces. On the electrode, the microspheres moved laterally until they approached the insulating rib. In the meantime, new individual particles continued to deposit in the groove (Figure 5b–d). In contrast to electrodeposition on nonpatterned substrates, the growth of the microbead clusters started from the wall (or from the two walls), as is shown in parts e and f of Figure 5. The new particles approaching the growing clusters moved along their periphery until they reached the position corresponding to the hexagonal structure. When the 2D colloid crystals nucleated at the two walls, they grew toward each other and merged in the center of the groove. In a rarely encountered scenario, the positions of the beads in the crystalline arrays propagating across the groove were commensurate with their positions in the hexagonal lattice; thus no structural rearrangement occurred in the

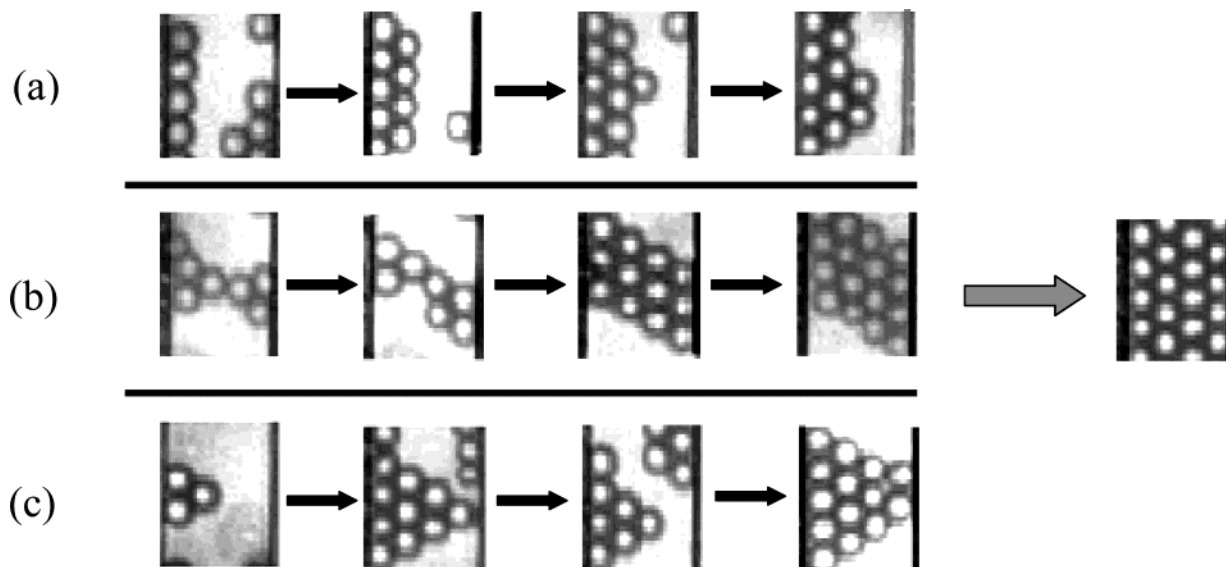


Figure 6. Different scenario in colloid crystal growth during electrodeposition in conductive grooves whose width is commensurate with two-dimensional lattice.

merging arrays. Generally, however, the positions of the beads in the two opposite arrays were incommensurate with the 2D lattice, as pointed with an arrow in Figure 5f. In this case, a cluster(s) underwent a small lateral displacement (Figure 5g) to generate a close-packed 2D lattice.¹⁸

Figure 6 shows several possible scenarios of 2D colloid crystallization in a constrained geometry. In Figure 6a the growth of colloid crystal in the groove occurs from a single wall. The new beads depositing in the groove and moving laterally across it are added to the growing cluster until it reaches the opposite wall. Figure 6b demonstrates the “bridgelike” formation of a colloid crystal. In this case, tiny arrays containing one to three particles grow toward each other until they form a bridge across the groove. At the beginning, such bridges do not necessarily have an ordered structure; small clusters, however, have sufficient mobility to rearrange upon merging. Further crystal growth occurs by the addition of new beads to the existing bridge. Finally, colloid arrays grow toward each other from the opposite ridges and merged in the middle of the groove (Figure 6c). Given sufficient electrodeposition time, all three processes resulted in the formation of a 2D close-packed array filling the channel.

Along the grooves, the 2D clusters containing from ca. 10 to 20 particles (depending on the concentration of particles in the dispersion) merged, undergoing small rearrangement to form a longer ordered array. When the clusters growing along the groove were too long, their structural rearrangement was hindered, and a grain boundary appeared between the two ordered domains of the resulting cluster. This problem was generally overcome by increasing the rate of electrodeposition or the concentration of particles in the dispersion.

By contrast with other methods, colloid crystallization occurred prior to drying of the colloid array. After 300 s of deposition, the conductive grooves were covered with the microbeads; the transparency of the substrates decreased and it became nearly impossible to continue to visualize the in situ experiments.

(18) We carried out experiments without colloid particles to find the nature of spherical inclusions appearing on the photoresist ridges. These experiments showed that small air bubbles (appearing presumably as a result of partial electrolysis of water) rise toward the upper surface (anode) and stick to the nonpolar ribs.

Discussion

The role of electric field in colloid crystal growth was 2-fold: it drove the charged microspheres toward the oppositely charged electrode and assisted in particle crystallization. The critical electric field bringing the particles to the electrode was determined by the relationship between the rate, V_s , of particle sedimentation under gravity and the rate of electrodeposition, V_e ¹⁹

$$V_e = \frac{\epsilon\epsilon_0\zeta}{\eta} E \quad (2)$$

$$V_s = \frac{2R^2\Delta\rho g}{9\eta} \quad (3)$$

where ϵ and ϵ_0 are the dielectric constants of the medium and the particles, ζ is the electrokinetic potential, E is electric field, η is the viscosity of the liquid medium, $\Delta\rho$ is the difference in densities of the particle and the liquid, and g is gravitational acceleration. For electrodeposition to occur $V_e > V_s$ and the critical electric field E_{cr} is

$$E_{cr} = \frac{2R^2\Delta\rho g}{9\epsilon\epsilon_0\zeta} \quad (4)$$

For $R = 1.94 \times 10^{-4}$ cm, $\Delta\rho \approx 0.1$ g/cm, $g = 980$ cm/s², $\epsilon \approx 40$, $\epsilon_0 = 1/4\pi$ esu² erg⁻¹ cm⁻¹, $\zeta = -20$ mV, and $\eta = 1.15$ cP, $E_{cr} \approx 1$ V/cm (for 5 μ m size spheres $E_{cr} \approx 1.6$ V/cm). Here, in a typical experiment a significantly stronger electric field of $E = 40$ V/cm was used to increase the velocity, $v = V_e - V_s$, of particle motion toward the electrode. Indeed, the time of particle migration over 0.25 cm (half of the distance between the electrodes) was ca. 80 and 2.8×10^4 s for electric field 40 and 1 V/cm, respectively.

The second function of the electric field was in generating lateral attraction between the microbeads deposited on the electrode surface. Lateral attraction exceeded electrostatic repulsion between the similarly charged particles and normal attraction between the particles and the surface. Attraction between the similarly charged

(19) Vold, R. D.; Vold, M. J. *Colloid and Interface Chemistry*; Addison-Wesley Publishing Company, Inc.: Reading, MA, 1983.

beads electrodeposited on nonpatterned electrodes surface has been reported by several groups.^{14–16} The origin of attraction was explained by the electroosmotic flow of the fluid near the charged nonconducting particle directed away from the electrode^{15a} or flow generated by the nonuniformity of “concentration polarization”²⁰ (caused by the particles deposited on the electrode). In either case, when two particles deposited on the electrode or when two small clusters formed on the electrode surface, the streamlines of liquid flow in the gap between the beads (directed away from the electrode) resulted in interparticle attraction. Since lateral attraction could be tuned by electric field, electrodeposition on nonpatterned substrates resulted in formation of reasonably well-ordered colloid arrays.^{4,14–16} Nevertheless, these arrays still had a multi-domain structure, in agreement with our observations.

In contrast, 2D colloid crystals obtained on patterned surfaces featured enhanced particle ordering, although the width of colloid arrays (determined by the width of the groove) was significantly smaller than the average dimensions of the domains formed on nonpatterned surfaces. In comparison with microbead assembly on blank ITO substrates, on patterned electrodes the nucleation and growth of colloid crystals occurred at the insulating wall. Particle motion toward the rigid wall was caused by the lateral flow of fluid near the wall and then away from the anode—in a manner similar to fluid flow near charged nonconducting particles.^{14–16} A particle that has deposited in the groove was thus convected toward the ridge.

The enhanced colloid crystallization on patterned substrates originated from the control of cluster size. In contrast to nonpatterned substrates, smaller 2D clusters retained their mobility and could undergo structural rearrangement when they came in contact. The width of clusters was controlled by the width of the groove. Since the number of columns (Figure 3) did not exceed five, across the groove the number of particles was smaller than in clusters immobilized on nonpatterned substrates.

Along the wall, colloid crystallization was enhanced for short clusters which merged undergoing structural rearrangement. Small clusters were formed when the time, t_{p-w} , taken by the microbead to approach the wall was shorter than the time of formation of particle clusters, t_{p-p} . The values of t_{p-p} and t_{p-w} were estimated using the approach of Solomentsev et al.¹⁵ in assumption that in both cases particle motion was driven by electroosmotic flow. The time, T , of particle motion over distance b was given by

$$T = \frac{(2(b/2)^2)^{1/2} - 2}{V_a} \quad (5)$$

where b is the initial spacing between the two clustering particles or the distance between the particle and the wall, normalized by the particle radius. The mean velocity V_a of the moving particle was given by¹⁵

$$V_a = 0.7322e^{-0.2766b} \quad (6)$$

The time of particle motion from the middle of the groove ($b = L/2R$) toward the wall with velocity $V_a = V_{p-w}$ is

$$t_{p-w} = \frac{\left(2\left(\frac{L/2}{2R}\right)^2\right)^{1/2} - 2}{V_{p-w}} \quad (7)$$

For particle–particle clustering, the particle–particle spacing, $b = d_{p-p}/R$ decreases with area fraction, α , covered

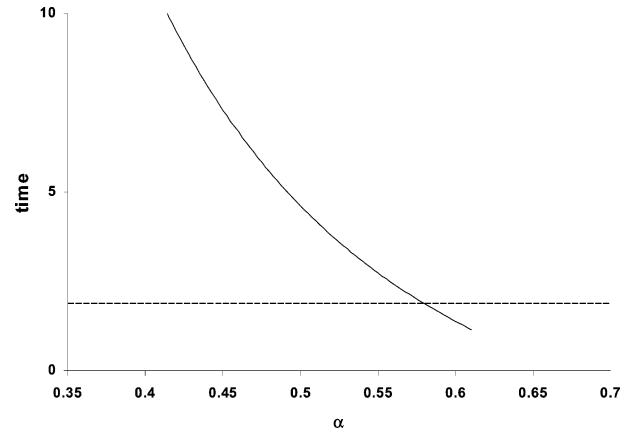


Figure 7. The variation of time of particle–particle clustering, t_{p-p} (—), and particle–wall motion, t_{p-w} (---), plotted as a function of surface coverage α . Note that $t_{p-p} = t_{p-w}$ at $\alpha = 0.58$.

by the particles as¹⁵

$$d_{p-g}/R = (5\pi/\alpha)^{1/2} - 2 \quad (8)$$

and

$$t_{p-p} = \frac{\left(2\left(\frac{(5\pi/\alpha)^{1/2} - 2}{2}\right)^2\right)^{1/2} - 2}{V_{p-p}} \quad (9)$$

where $V_{p-p} = V_a$ is the mean velocity of particle clustering and t_{p-p} is the time of particle clustering.

In eq 8 and eq 9 the values of V_{p-w} and V_{p-p} depend on the particle–particle or particle–wall spacing and are given by eq 7. Figure 7 shows the dimensionless time of particle–particle and particle–wall motion for $L/2R = 3.56$. Particle–particle clustering begins to dominate only for $\alpha > 0.58$; thus the formation of small and mobile clusters is favored, which in turn results in enhanced colloid crystallization.

The role of commensurability and particle polydispersity was consistent with our previous work: larger than ca. 15% mismatch between $L/2R$ and $L/2R_{exp}$ resulted in defects in 2D hexagonal lattice. Figure 4b, however, indicated that a larger mismatch between the groove width and the particle size is possible when the groove height is substantially smaller than particle radius. This effect was similar to colloid assembly through the electrostatically driven attraction between the particles and the oppositely charged surface domains,^{6b,c} and it is not the scope of this paper. We believe, however, that lack of physical confinement reduced the extent of order in the colloid arrays.

In summary, the results of in situ studies of colloid crystallization in confined geometry provided further insight into the nature of this approach. Following particle electrodeposition on the patterned electrode, colloid crystal growth occurred through nucleation and growth at the groove wall. Confinement of the colloid arrays reduced the size of particle clusters. Small clusters easily underwent structural rearrangements to produce close-packed crystals when the groove width was commensurate or nearly commensurate with the 2D lattice. Incommensurability exceeding ca. 15% produced distorted colloid arrays.

LA030145U

(20) Levich, V. G. *Physicochemical Hydrodynamics*; Prentice-Hall: Englewood Cliffs, NJ, 1962.